Supplement of Atmos. Chem. Phys., 21, 13443–13454, 2021
https://doi.org/10.5194/acp-21-13443-2021-supplement

Atmospheric Chemistry and Physics
Open Access
EGU

Supplement of

Characteristics of surface energy balance and atmospheric circulation during hot-and-polluted episodes and their synergistic relationships with urban heat islands over the Pearl River Delta region

Ifeanyichukwu C. Nduka et al.

Correspondence to: Steve Hung Lam Yim (yimsteve@gmail.com)

1 Introduction

The texts, figures and tables provide additional information that will help in our understanding of the model configuration, model evaluation and HPE identification and characterization.

1.1 Details of WRF model configurations

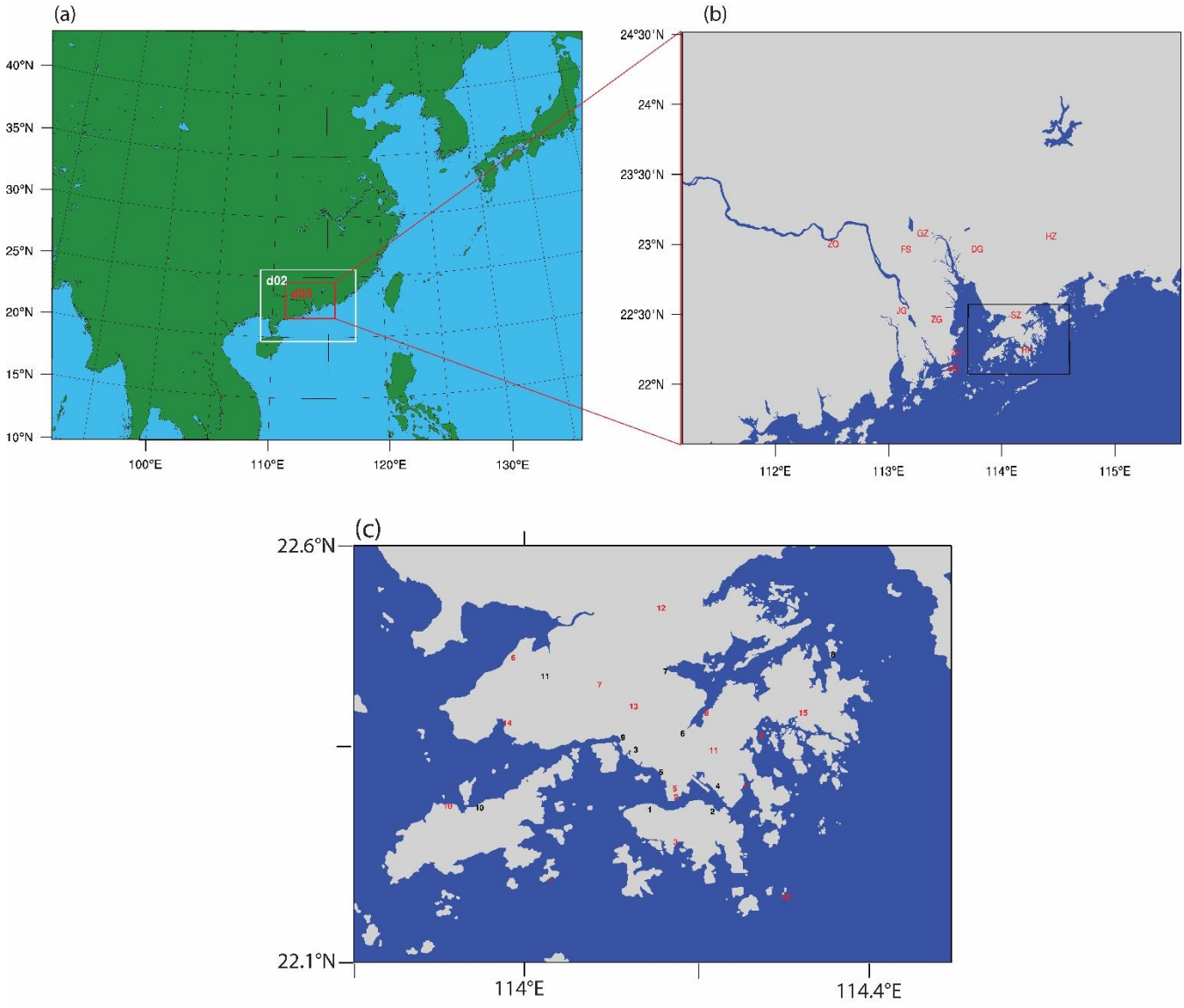

Figure S1. (a) WRF-Chem simulation domains. Downscaling was performed from D1 (27 km), D2 (9 km), and then D3 (3 km). (b) The study area and the location of all the cities in the study area (GZ – Guangzhou, SZ – Shenzhen, FS - Foshan, DG - Dongguan, ZG - Zhongshan, ZH - Zhuhai, HZ - Huizhou, JG - Jiangmen, ZQ – Zhaoqing, HK - Hong Kong, MC - Macau). The black box shows the Hong Kong area where the observation stations are located. (c) The air quality stations are numbered in black, while the meteorology stations are numbered in red). More information about the stations is presented in section 2.

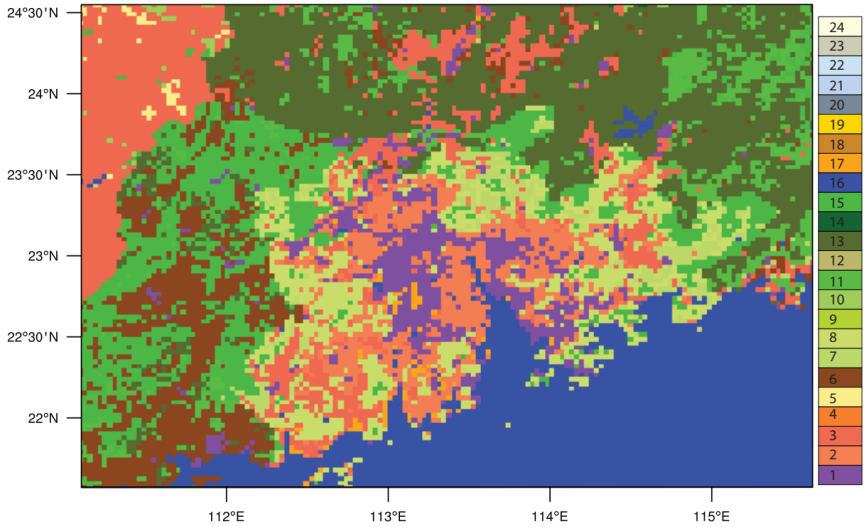

Figure S2. WRF Domain 3 USGS LULC configuration. USGS categorizations are named as follows: 1 Urban and Built-Up; 2 Dryland, Cropland, and Pasture; 3 Irrigated Cropland and Pasture; 4 Mixed Cropland and Pasture; 5 Cropland/Grassland Mosaic; 6 Cropland/Woodland Mosaic; 7 Grassland; 8 Shrubland; 9 Mixed Shrubland/Grassland; 10 Savanna; 11 Deciduous Broadleaf; 12 Deciduous Needleleaf; 13 Evergreen Broadleaf; 14 Evergreen Needleleaf; 15 Mixed Forest; 16 Water Bodies; 17 Herbaceous Wetland; 18 Wooded Wetland; 19 Barren/Sparsely Vegetated; 20 Herbaceous Tundra; 21 Wooded Tundra; 22 Mixed Tundra; 23 Bare Ground Tundra; 24 Snow or Ice.

Table S1. Details for the WRF configurations used in this study.

Configurations	**Physics scheme options**
Microphysics	Morrison 2-Moment Scheme
Longwave Radiation	RRTMG Longwave Scheme
Shortwave Radiation	RRTMG shortwave Scheme
Surface Layer	MM5 Similarity Scheme
Land Surface	Unified Noah Land Surface Model
Planetary Boundary Layer	YSU
Cumulus	Grell 3D Scheme

In the innermost model domain (Figure S1a), the urban areas were also found to aggregate toward each other and comprised 11 cities located in the PRD region (Figure S1b: Guangzhou, Shenzhen, Foshan, Dongguan, Zhongshan, Zhuhai, Huizhou, Jiangmen, Zhaoqing, Hong Kong, and Macau. Table S1 shows the physics schemes used in the model simulations. The chemical mechanism option was set as CB05 and a MADE/SORGAM_aq aerosol model was used. The USGS land use/land cover categorization from WRF was used to delineate between urban/built-up and vegetated areas. The urban and built-up category was used to represent urban surfaces and the vegetated category represented all other surfaces besides urban and

water categories (Figure S2). The data shows that about 15% and 70% of the domain was designated as built-up and vegetated land use, respectively.

2 Model Evaluation

2.1 Evaluation method

The results from the baseline model simulations were compared with observations from stations within the PRD region (Figure S1b; 16 stations for meteorology and 11 for air quality). Metrics used to validate the performance of the model included correlation coefficients (r), mean bias (MB), root mean squared error (RMSE), and Index of Agreement (IoA), the mathematical expressions for which are

$$r = \frac{\sum_{i=1}^{N}(M_i-\bar{M})\cdot(O_i-\bar{O})}{\sqrt{\sum_{i=1}^{N}(M_i-\bar{M})^2}\cdot\sqrt{\sum_{i=1}^{N}(O_i-\bar{O})^2}} \quad (1)$$

$$\mathrm{MB} = \frac{1}{N}\sum_{i=1}^{N}(M_i - O_i) \quad (2)$$

$$\mathrm{RMSE} = \sqrt{\frac{1}{N}\sum_{i=1}^{N}(M_i - O_i)^2} \quad (3)$$

$$\mathrm{IOA} = 1 - \frac{\sum(M_i-O_i)^2}{\sum(|M_i-\bar{O}|+|O_i-\bar{O}|)^2} \quad (4)$$

where M_i and O_i are values of the model and observation results at hour i, respectively; N is the number of samples (hours) for each time and location; and $\overline{M}$ and $\overline{O}$ are model and observation means, respectively.

2.2 Model performance

Table S2a. Model evaluation for mean air temperature at 2 m (T_2), wind speed at 10 m (WS_{10}), and relative humidity at 2 m (RH_2) for all eight HPEs and 16 stations. RMSE, root mean square error, MB, mean bias.

Statistical Variables	T2 (°C)	WS_{10} (m/s)	RH_2 (%)
Model Mean	28.31	4.23	75.67
Observation Mean	28.08	3.40	76.57
Correlation Coefficient	0.70	0.33	0.64
RMSE	1.94	2.67	10.25
MB	0.25	0.86	-1.07

Table S2 shows the results for model evaluation. The simulated means of all the variables were consistent with the observed means. Strong correlations were found between model results and observations for T_2 and RH_2 with correlation coefficients of 0.70 and 0.64, respectively. The MB and RMSE for T_2 were 0.25°C and 1.94°C, respectively. For RH_2, MB and RMSE were −1.07% and 10.25%, respectively. The correlation coefficient for wind speed was approximately 0.33, whereas the MB and RMSE were 0.86 and 2.67 m/s, respectively. These results indicate an overestimation of surface wind speeds in the WRF model, which is reported to be a common problem in regional meteorological modelling (Fan et al., 2011). A possible reason for this is that the observations represent wind speed at one local point, whereas the results for the model represent an average quantity over a model grid. The T_2 and RH results indicate good agreement between the simulated results and the observations. Overall, the evaluation results show that the WRF model was sufficiently robust for this study.

Table S2b. Model evaluation for mean $PM_{2.5}$, PM_{10}, Ozone (O_3), Nitrogen di oxide (NO_2), and Sulfur di oxide (SO_2) for all eight HPEs and 11 stations. RSME, root square mean error, mean bias; Model mean; Observation (Obs) Mean; Index of Agreement.

Statistical Variables	$PM_{2.5}$	PM_{10}	O_3	NO_2	SO_2
Model mean	15.5	28.0	37.3	37.4	15.5
Obs Mean	32.0	44.3	46.5	50.5	14.6
Index of Agreement	0.5	0.5	0.6	0.6	0.6
RMSE	23.8	27.5	46.7	31.3	15.3
Mean Bias	-17.6	-16.3	-4.8	-8.1	0.9

The air quality evaluation was conducted for $PM_{2.5}$, PM_{10}, O_3, NO_2 and SO_2. The mean result from the 11 stations and 8 HPEs studied shows that the index of agreement was 0.5 and 0.6 for the particulates and gaseous, respectively. The mean bias for the particulates were -17.6 µg/m^3 ($PM_{2.5}$) and -16.3 µg/m^3 (PM_{10}), while the gases were -4.8 µg/m^3 (O_3), -8.1 µg/m^3 (NO_2) and 0.9 µg/m^3 (SO_2). The underestimation observed for the particulates can be attributed to the overestimation of wind speed which can result in increased dispersion and lowering of concentrations.

.

105

3 Identified HPEs

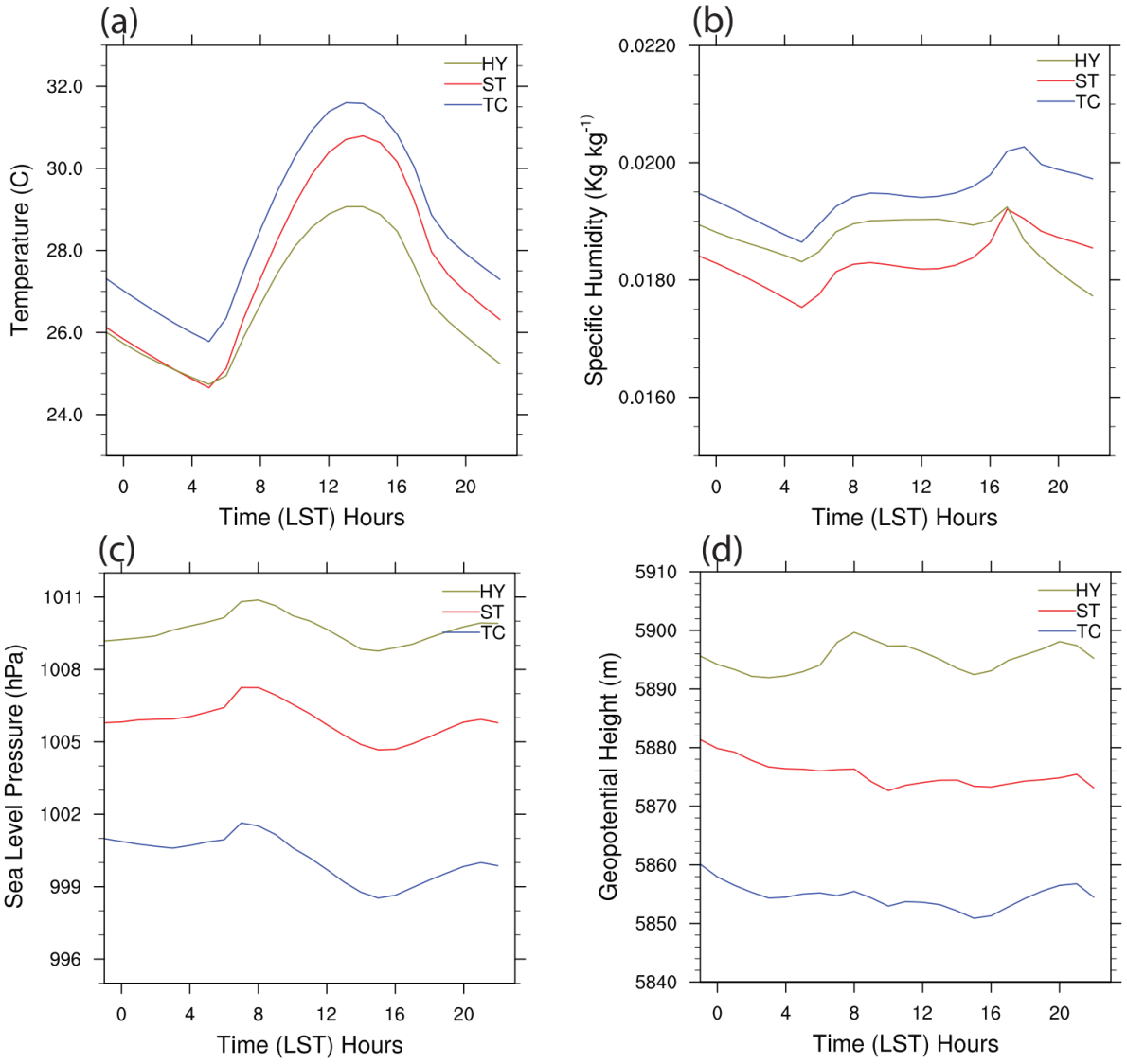

Figure S3. (a) Air temperature at 2 m (T_2). (b) Specific humidity. (c) Sea level pressure. (d) Geopotential Height. Diurnal means are for the three clusters for TC (blue lines), ST (red lines), and HY (brown lines) group.

110 The results of the cluster analysis indicate that eight HPEs can be classified based on their formation and characteristics: Tropical Cyclone (TC-HPE); Stagnant (ST-HPE); and Hybrid (HY-HPE). Figure S3 showed the diurnal means of T_2, specific humidity, Sea Level Pressure (SLP), and geopotential height of the three HPE groups. Particularly, T_2 among the HPEs in each

group did not vary significantly, whereas remarkable differences were found in T_2 among the three groups. The TC-HPE had the highest temperature (32 °C) during its peak period, followed closely by the peak of ST-HPE (31 °C) and HY-HPE (29 °C), which typically occurred at 14:00 local time. Among the three groups, TC-HPE had a relatively lower SLP (~999 hPa) and geopotential height (GPH, 5,855 m), whereas for ST-HPE and HY-HPE, these values were respectively approximately 1,005 hPa and 5,875 m and approximately 1,009 hPa and 5,895 m (Figure S3c-d).

4 Weather Charts of HPE group

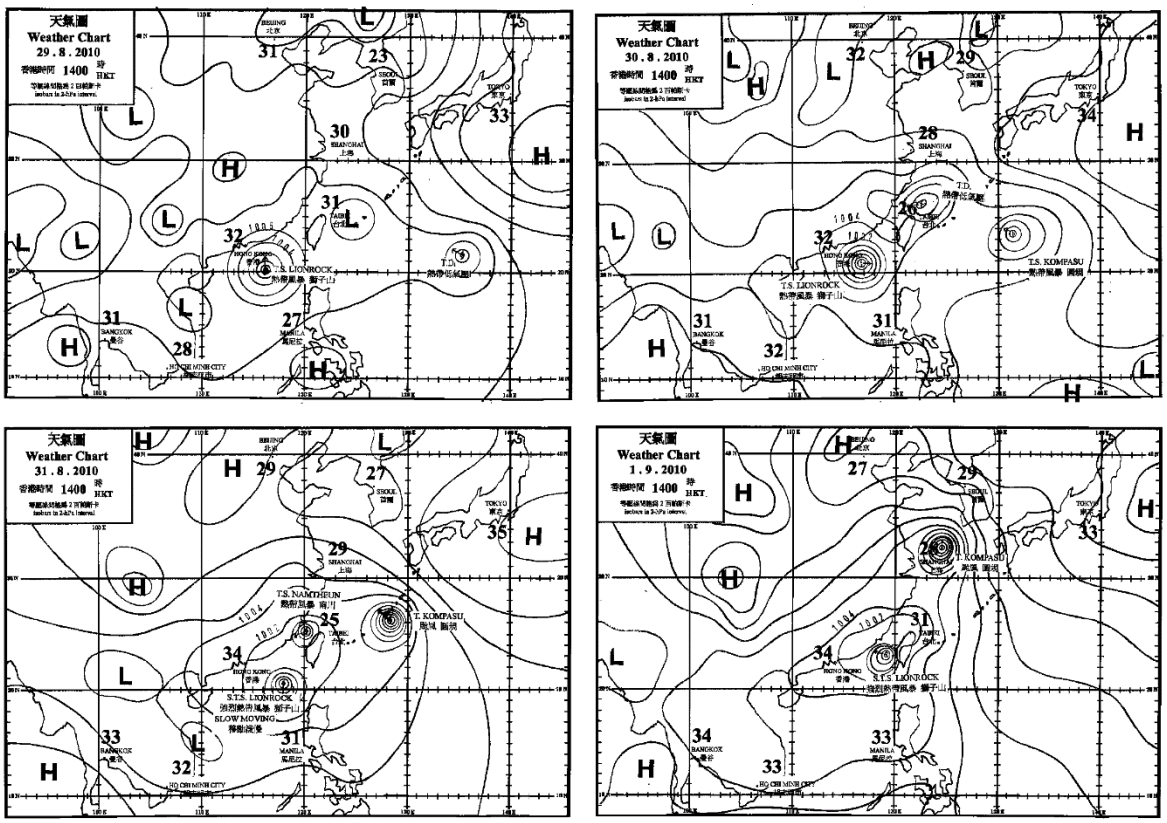

Figure S4: Tropical cyclone group Episode (20100829-0901) Shows the evolution of the temperature and pressure conditions during the TC-HPE. The weather charts were obtained from the Hong Kong Observatory web site (https://www.hko.gov.hk/en/wxinfo/currwx/wxcht.htm) on may. 2018.

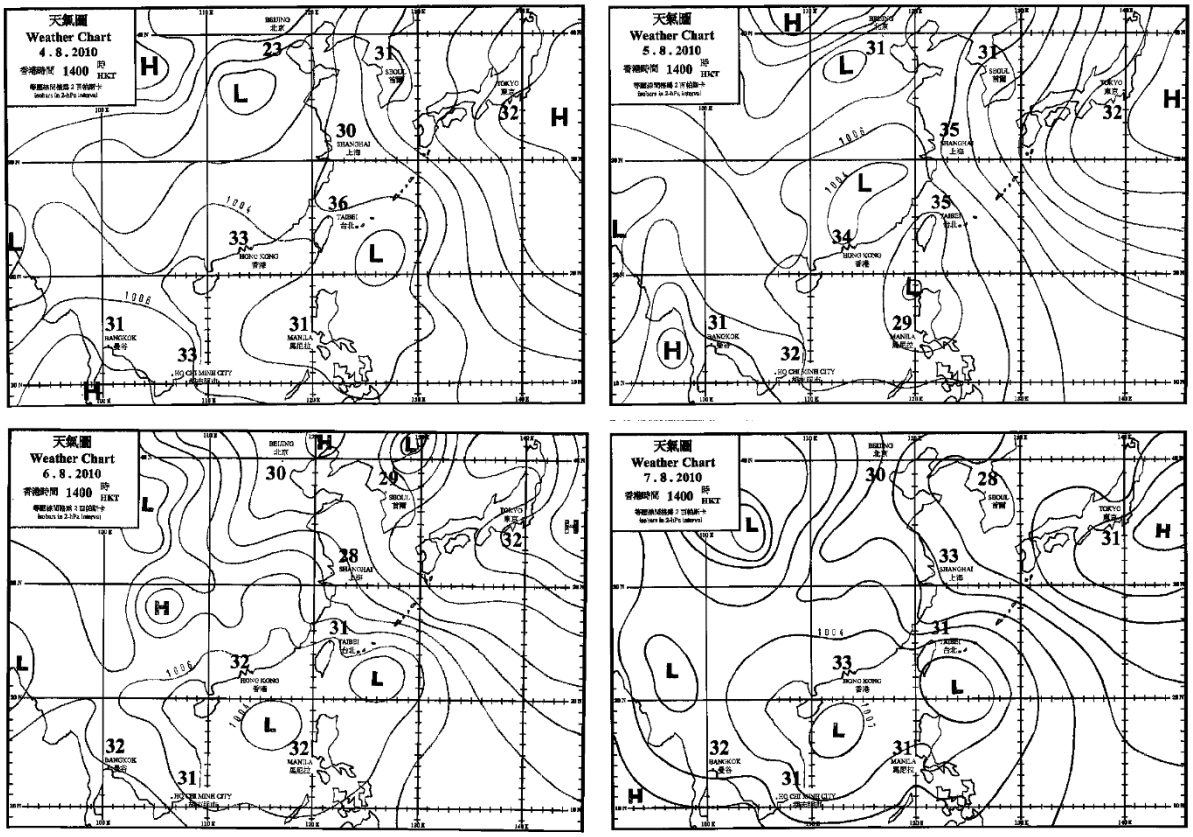

Figure S5: Stagnant group Episode (20100804-07) Shows the evolution of the temperature and pressure conditions during the ST-HPE. The weather charts were obtained from the Hong Kong Observatory web site (https://www.hko.gov.hk/en/wxinfo/currwx/wxcht.htm) on may. 2018.

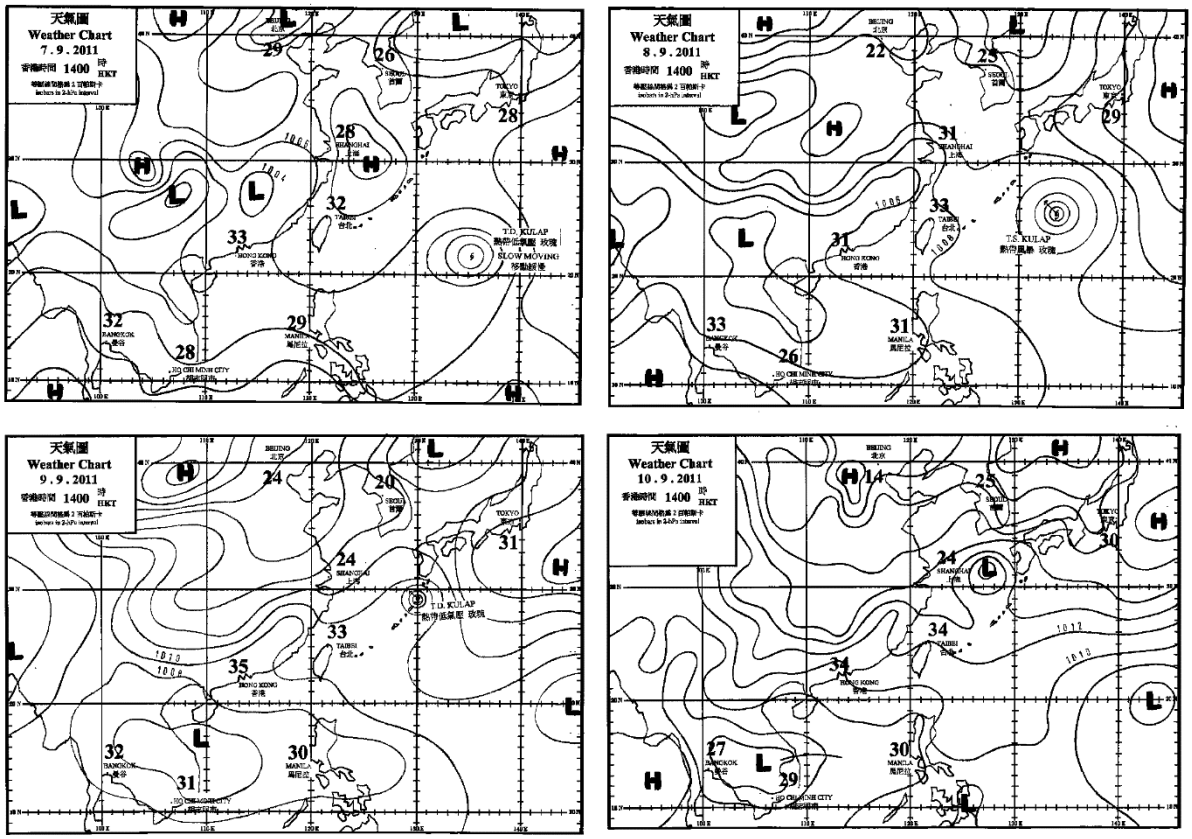

135 Figure S6. Hybrid group Episode (20110907-10) Shows the evolution of the temperature and pressure conditions during the HY-HPE. The weather charts were obtained from the Hong Kong Observatory web site (https://www.hko.gov.hk/en/wxinfo/currwx/wxcht.htm) on may. 2018.

5 Simulated Wind profiles for the HPE groups

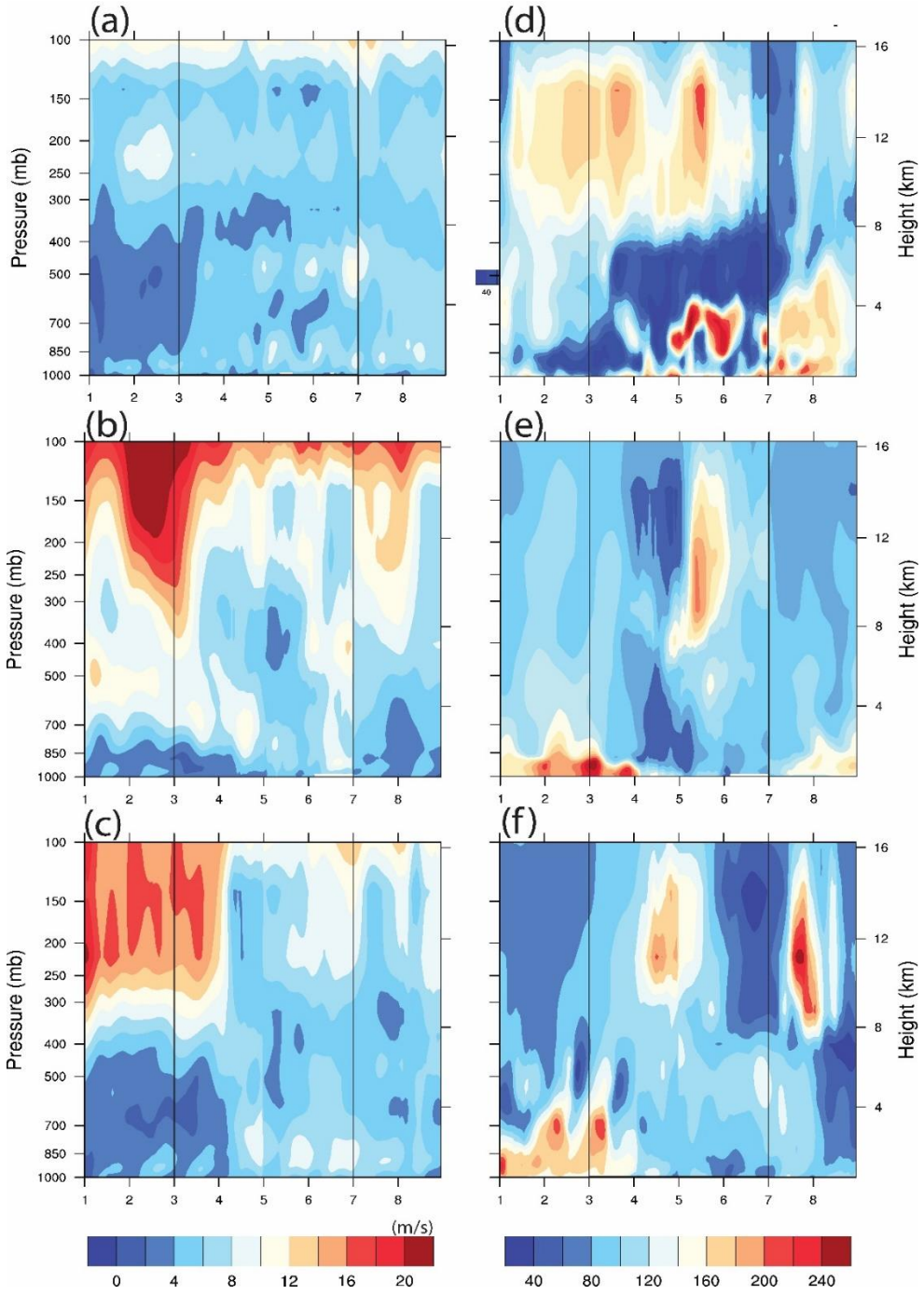

Figure S7. (a-c) Wind speed(m/s) for TC-HPE, ST-HPE and HY-HPE; (d-f) Wind direction for TC-HPE, ST-HPE and HY-HPE. Black boxes represent the period of HPEs.

References

Chan, E. Y. Y., Goggins, W. B., Kim, J. J. and Griffiths, S. M.: A study of intracity variation of temperature-related mortality and socioeconomic status among the Chinese population in Hong Kong, J Epidemiol Community Health, 66(4), 322–327, doi:10.1136/jech.2008.085167, 2012.

Fan, S. J., Fan, Q., Yu, W., Luo, X. Y., Wang, B. M., Song, L. L. and Leong, K. L.: Atmospheric boundary layer characteristics over the Pearl River Delta, China, during the summer of 2006: measurement and model results, Atmospheric Chemistry and Physics, 11(13), 6297–6310, doi:https://doi.org/10.5194/acp-11-6297-2011, 2011.

Wang, Y., Chan, A., Lau, G. N.-C., Li, Q., Yang, Y. and Yim, S. H. L.: Effects of urbanization and global climate change on regional climate in the Pearl River Delta and thermal comfort implications, International Journal of Climatology, 39(6), 2984–2997, doi:10.1002/joc.5996, 2019.